ELSEVIER

Polymer 43 (2002) 4487–4493

polymer

www.elsevier.com/locate/polymer

Role of thermal history on quiescent cold crystallization of PET

Z. Kiflie[a], S. Piccarolo[a,*], V. Brucato[b], F.J. Baltá-Calleja[c]

[a]*Dipartimento di Ingegneria Chimica dei Processi e dei Materiali, DICPM, Università di Palermo, Viale delle Scienze, 90128 Palermo, Italy*
[b]*Dipartimento di Ingegneria Chimica e Alimentare, Università di Salerno, DICA, Viale ponte don Melillo 84084, Fisciano (SA), Salerno, Italy*
[c]*Instituto de Estructura de la Materia, CSIC, Serrano 199, 28006 Madrid, Spain*

Received 22 January 2002; received in revised form 3 April 2002; accepted 8 April 2002

Abstract

The cold crystallization of poly(ethylene terephthalate) (PET) has been studied as a function of the initial structure of the glass using density, microhardness, wide angle X-ray scattering, small angle X-ray scattering and DSC measurements. Glassy PET samples varying from slightly crystalline to completely amorphous phase were investigated. Results reveal that differences in the inner structure of the starting glassy material induce different crystallization rates from the glassy amorphous state. Thus, it is observed that crystallization rate decreases with the increasing cooling rate used to quench the samples. Results have been analyzed using the Kolmogroff–Avrami–Evans theory. A good agreement between theoretical and experimental data is obtained providing accurate values for kinetic constants. The different crystallization rates obtained are explained in terms of differences in nucleation density.

Keywords: Poly(ethylene terephthalate); Cold crystallization; Isothermal

1. Introduction

Isothermal crystallization of polymers is commonly used to investigate the specific mechanisms of the crystallization processes. From a theoretical point of view it is easier to analyze than non-isothermal crystallization. Isothermal crystallization can be carried out either from the melt or, for slowly crystallizing polymers like poly(ethylene terephthalate) (PET), from the glassy state. The isothermal crystallization study of PET is also relevant from a technical point of view, as it is frequently encountered in processing methods such as reheat stretch blow-molding of bottles, heat setting, production of films and fibers, etc. The physical and mechanical properties of such products are, directly or indirectly, controlled by the crystallization process. For this and other reasons its crystallization kinetics has been widely investigated.

A number of researchers have investigated the influence of various factors (crystallization temperature, catalysts, molecular weight, initial structure of the glassy polymer, etc.) on the crystallization kinetics of PET [1–5]. Bove et al. [6] analyzed the influence of ageing on the rate of the crystallization kinetics of PET at 120 °C using infrared spectra, wide angle X-ray scattering (WAXS) and polarized light microscopy. These authors reported that aged samples crystallize at a faster rate than the unaged ones, suggesting that this might be due to the presence of ordered domains in the aged samples which served as nuclei to the crystallization process.

Another important factor is the initial structure of the sample (morphology) prior to the cold crystallization process. In fact, the initial structure can be easily altered by the introduction of orientation to the sample with the consequent influence on the rate and extent of the subsequent crystallization process [7]. The role of the initial structure in unoriented glassy PET samples upon isothermal cold crystallization can be immediately appreciated in the reheat stretch blow-molding process used for the production of PET bottles. The initial structure of the preform must be such that the quenching used is so efficient that spherulitic crystallization is inhibited during the preheating and equilibration periods before the stretching stage. Apart from such a practice in the production sector, it may be said that not much has been documented concerning the influence of thermal history of glassy PET on cold crystallization. In addition, the quenching process is not always performed under the same conditions, and in common practice, it is not quantified.

In a preceding study, we showed that melt solidified PET undergoes a continuous structural modification with increasing cooling rates [8] in which:

(i) at very high cooling rates (>100 °C/s), a completely

* Corresponding author. Tel.: +39-91-6567225; fax: +39-91-6567280.
E-mail address: piccarolo@unipa.it (S. Piccarolo).

0032-3861/02/$ - see front matter
PII: S0032-3861(02)00260-4

amorphous structure is characterized by the asymptotic value of density and by the constancy of the long period.
(ii) at cooling rates lower than 2 °C/s, a semicrystalline structure, as seen from WAXS, small angle X-ray scattering (SAXS), and DSC analysis is evidenced, in which density and microhardness were observed to change very slowly with cooling rate.
(iii) at intermediate cooling rates a metastable or a precrystalline phase is obtained.

A precrystalline state (neither crystalline nor amorphous) has been evidenced by the absence of crystalline reflections in the WAXS patterns and the occurrence of SAXS maxima [9] and exothermic peak areas (DSC) in the cooling rate range above 2 °C/s [8]. The internal order of the amorphous state of PET has also been characterized using the microhardness technique [10]. Here the hardness contribution to physical ageing as well the influence of cooling rate upon hardness have been discussed. Thus, it is possible to expect structural differences between these non-crystalline samples depending on the cooling rates used.

The aim of the present report is to extend the above investigations and to systematically study the influence of the initial structure of the quenched material on the kinetics of cold crystallization, as revealed by X-ray scattering, microindentation hardness and DSC techniques.

2. Experimental

2.1. Materials

The material used in this study was a fiber grade PET resin having an intrinsic viscosity of 0.62 dl/g, M_w 39,000, kindly supplied by Mossi & Ghisolfi Group. Intrinsic viscosity (IV) was measured in a solution of phenol/tetrachloroethane (60/40 w/w) at 30 °C at the Mossi & Ghisolfi Research Center of Pozzilli, Italy. The pellets were dried at 170 °C under vacuum for 7 h from which films of thickness ranging from 100 to 200 μm were compression molded under vacuum.

Glassy PET samples with different thermal histories (Table 1) were prepared by melt solidifying the films at controlled cooling rates using the cooling technique described in Ref. [8].

Isothermal crystallization was carried out by immersing the samples in an agitated thermal bath filled with silicon oil kept at 100 ± 0.2 °C. Samples were immediately quenched, always at the same cooling rate, in an ethylene glycol bath maintained at −25 °C at the end of specified crystallization times. Thereafter, the samples were analyzed by density, microhardness, WAXS and SAXS. This procedure was followed mainly because it was difficult to apply time resolved measurements for density and microhardness. For density measurements, the gradient column technique could not be used since it was not possible to isolate mutually miscible solvents having sufficiently small vapor pressure at 100 °C and that are not harmful to the polymer studied. To our knowledge, even fluorocarbons do not comprise a solvent pair with a density range from 1.3 to 1.4 g/cm^3.

Table 1
Parameters of the Avrami equation obtained from linear regression

Sample name	n	k'	k	$t_{1/2}$ (min)
Sample_2	1.6991	0.0857	0.1063	9.4
Sample_6	2.1934	0.0673	0.0796	12.6
Sample_11	2.2864	0.0600	0.0704	14.2
Sample_20	2.2253	0.0584	0.0689	14.5
Sample_150	2.5295	0.0400	0.0462	21.6
Sample_1500	2.393	0.0373	0.0435	23.0

2.2. Techniques

A gradient column filled with a solution of *n*-heptane and carbon tetrachloride with a resolution of 0.0001 kg/l and a repeatability within 0.0002 kg/l was used for density measurement at 25 °C. Each sample was properly checked against entrapped air bubbles using a microscope and afterwards degassed before being introduced into the column. An average of five samples were analyzed for each test condition.

Microhardness measurements were carried out using an MHT-10 Vickers indenter by Anton Paar. Peak forces of 0.1, 0.15 and 0.25 N were used to correct for instantaneous elastic recovery [11] and an average of five measurements were done with each force. The microhardness, H_v was calculated from the residual projected indented area using the relation

$$H_v = 2F\frac{\sin(\alpha/2)}{d^2} = 1.854\frac{F}{d^2} \quad (1)$$

where H_v is the microhardness in Pa, d is the mean diagonal length of the projected impression in meters and F is the peak force in Newton and a is the included angle between two non-adjacent faces (136° for the Vickers indenter).

WAXS measurements were carried out using a Bruker AXS D8 Advance X-ray diffractometer with nickel-filtered Cu Kα radiation. Patterns were subtracted with the background and FFT filtered. SAXS measurements were performed on the beam line A2 of the synchrotron radiation source at HASYLAB, DESY, Hamburg, Germany by a one-dimensional Gabriel detector placed at 1.9 m from the sample. The path between the sample and the SAXS detector was evacuated in order to reduce air scattering and absorption. The SAXS patterns have been normalized on the same relative scale and corrected for blank scattering and sample absorption by means of two ionization chambers placed before and after the sample, respectively. An oriented specimen of wet collagen (rat-tail tendon) has been used to calibrate the SAXS detector.

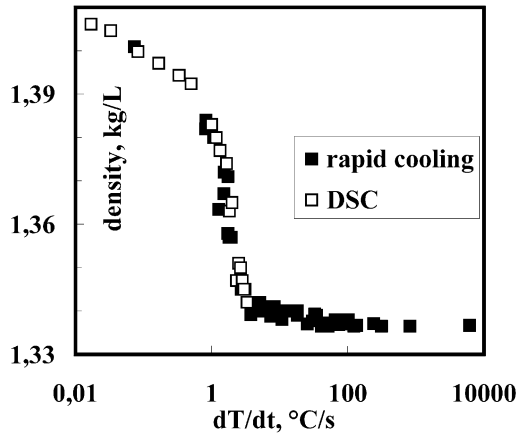

Fig. 1. Variation of macroscopic density as a function of cooling rate for PET samples.

3. Results and discussion

3.1. Characterization of the starting materials

Fig. 1 shows the variation of density with increasing cooling rate for melt solidified PET. Here it is possible to identify slow, very high, and small variations in density at low, intermediate and high cooling rates, respectively. A transition zone from the high to the low density region can be identified in the range between 0.8 and 3 °C/s.

Fig. 2 depicts the variation of the WAXS patterns, for the various melt quenched samples of PET, with the cooling rate. One sees that no crystalline reflections are detected in the WAXS spectra for cooling rates beyond ~2 °C/s. Only sample quenched at 2 °C/s eventually shows remnants of α-triclinic phase reflections. Fig. 3 shows that in the Lorentz-corrected SAXS patterns a scattering maximum

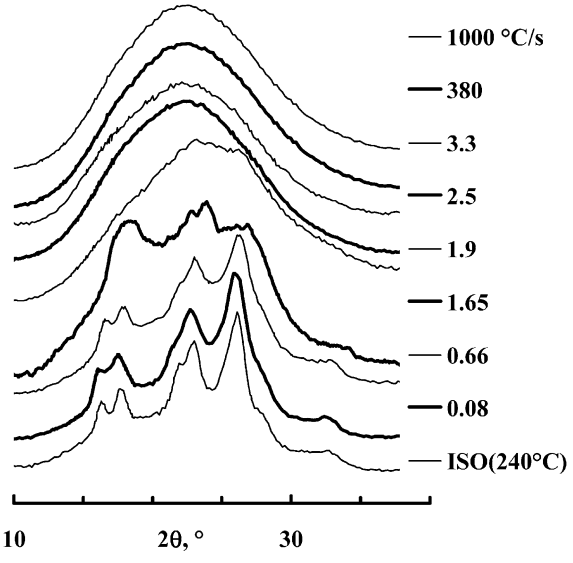

Fig. 2. X-ray diffractograms of PET cooled from the melt at different cooling rates, shown in the legend. Bottommost refers to isothermal DSC crystallized sample.

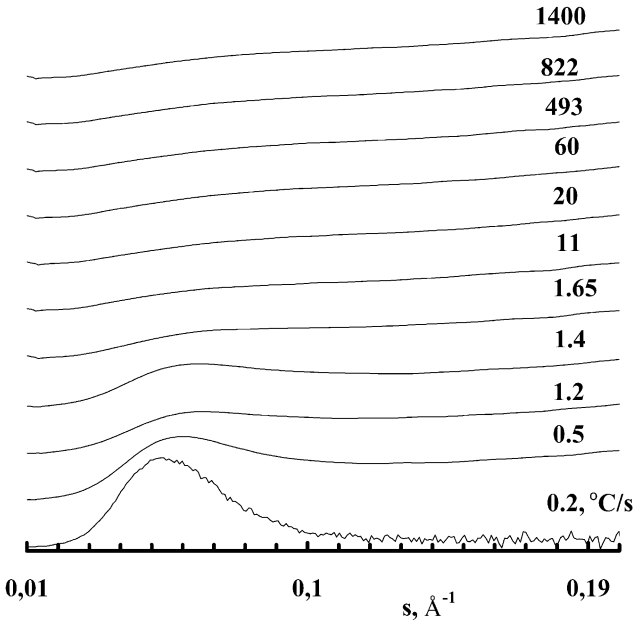

Fig. 3. Lorentz-corrected SAXS profiles of PET cooled from the melt at different cooling rates, shown in the legend.

already appears at relatively high cooling rates and continues to increase in intensity upon decreasing cooling rates before the first crystalline reflections in the WAXS spectra are detected. Preceding studies made on PET [12,13], have also shown that SAXS peaks appear before the formation of nuclei and their intensity increases before the WAXS maxima become visible. The increase in SAXS intensity can be associated with the increase in the electron density fluctuations in the polymer. One may, therefore, expect structural differences between these non-crystalline samples. The aim of this work is to analyze the influence of such structural differences on the cold crystallization of PET. The samples examined in the present study are all essentially non-crystalline and were prepared using cooling rates of 2, 6, 11, 20, 150, and 1500 °C/s, respectively.

3.2. Cold crystallization

Isothermal crystallization was followed by measuring density, microhardness and the WAXS patterns. However, these measurements were not performed in situ due to the cited experimental difficulties. Tests were made on samples originally quenched at different cooling rates. The samples were then quenched under identical conditions at the end of specified crystallization times. Such procedure gives rise to a cumulative propagation of errors arising from the complex thermal history the samples are subjected to before each measurement. The starting samples were all non-crystalline according to the WAXS patterns, i.e. no crystalline reflections were detected but for sample_2. The most significant difference between the samples lies on the cooling rate employed to obtain them. In other words, the different non-crystalline samples subject to the cold crystallization

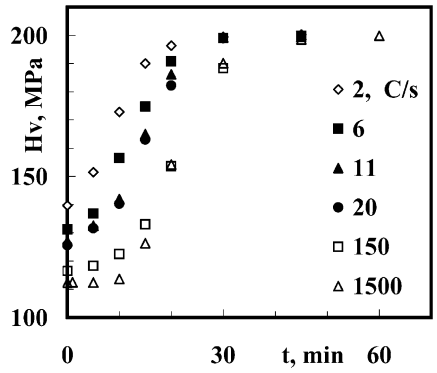

Fig. 4. Microhardness of the PET samples during isothermal crystallization at 100 °C vs. crystallization time.

study have undergone different thermal histories and, therefore show different internal order. Figs. 4 and 5 show the changes of microhardness and density with crystallization time for the different glassy PET samples, respectively. The microhardness and density variations show the typical profile of the isothermal crystallization processes; namely one observes a sigmoidal rapid increase of microhardness and density eventually followed by a very slow final increase.

The initial differences in microhardness and density observed ($t = 0$ in Figs. 4 and 5) are a result of differences in internal order and not to the presence of crystallinity but for sample_2 as already stated. However, in spite of the fact that the samples are essentially non-crystalline, they strikingly show different crystallization rates when subjected to cold crystallization (Figs. 4 and 5). For example, sample_2 (solidified at 2 °C/s) reaches the plateau value after ~20 min, while sample_1500 (solidified at 1500 °C/s) reaches the same value after about 60 min. Thus, with increasing cooling rate, a progressive reduction of the crystallization rate is encountered. A closer inspection of the above results indicates that the rate of crystallization becomes almost constant above ~100 °C/s. For example, sample_150 and sample_1500 show practically the same crystallization rate. In addition, it can be observed that

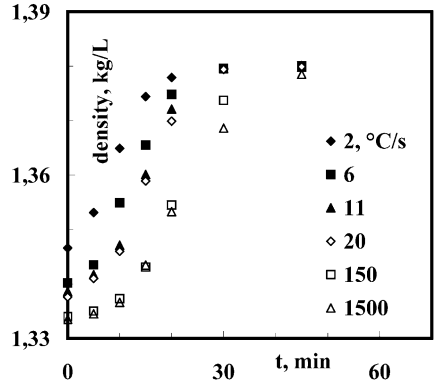

Fig. 5. Density of the samples of Fig. 4 during isothermal crystallization at 100 °C vs. crystallization time.

beginning of crystallization progressively delays from sample_2 to sample_150. It is also noteworthy, that all the samples reach the same plateau, both in density (1.38 kg/l) and microhardness (200 MPa), irrespective of the initial differences in thermal history; although a slight increase in density can be noted at longer times probably due to secondary crystallization effects. Finally, it can be concluded that the faster crystallization process (which with some caution one could identify with primary crystallization) is completed after 60 min even for the slowest crystallizing sample_1500.

3.3. Precrystalline order

At this stage, one may ask, why the above PET samples crystallize at different rates in spite of being essentially non-crystalline. This finding suggests that the degree of internal order for each amorphous phase is different from the other. We have pointed out before that the structural modification of PET with cooling rate is a gradual one. PET samples quenched from low to very high cooling rates are useful traces of the gradual transformation of PET. Preceding results show that the time scale for electron density fluctuations prior to cold crystallization of PET strongly depends on the local arrangement of polymer chains within the glassy state induced by different heat treatments of the starting material [14]. Especially, the very highly quenched samples resemble the early stages of crystallization process that have been observed in Ref. [15]. With decreasing cooling rate, PET gradually transits from a disordered state to a state of long range order, finally leading to the formation of crystals. Hence, it is possible to freeze-in the different stages of the crystallization process, even the very early stages by using appropriate cooling rates. Therefore, based on this concept the samples subjected to cold crystallization experiments, although essentially non-crystalline, should show inherent structural differences. These samples cover quite a wide range of cooling rates. Thus, on the one extreme, the structure of sample_1500 is very close to the completely amorphous phase and on the other extreme, the structure of sample_2 should be closer to the beginning of crystal formation. By comparing only the initial structures, it can be said that sample_2 is closer to the crystalline phase than is sample_1500 because there is a higher precrystalline order in the former than in the latter. Hence, the differences in crystallization rate observed between these samples during isothermal cold crystallization could be explained in terms of these inherent structural differences giving rise to crystal precursors or what we shall call physical cross-links.

3.4. Kinetics of crystallization: KAE model

The sigmoidal form of the curves in Figs. 4 and 5 can be explained by applying the theory of Kolmogoroff–Avrami–Evans (KAE) [16–18]. This model has been sometimes criticized [19] because the deviations encountered between

the model and experimental data have been attributed to various simplifying assumptions. In this model one takes into account the impingement of morphological units like spherulites with a statistically distributed nucleation center. One then obtains

$$\frac{(1 - X_{rel})}{(1 - X_{rel,0})} = \exp[-\ln 2 \times (kt)^n] = \exp[-(k't)^n] \quad (2)$$

where $X_{rel} = X_t/X_{max} = (\rho_t - \rho_a)/(\rho_{max} - \rho_a)$ is the relative crystallinity and ρ_a is the value of the amorphous density that is not constant, but is a function of thermal history, and X_t and ρ_t are the crystallinity and the density at time t, respectively. The term X_{max} is the crystallinity corresponding to the maximum value of the density, ρ_{max}, at the end of the crystallization process.

As has been already noted, initially the samples do not show any crystalline reflections in the WAXS patterns. Therefore, $X_{rel,0}$ can be correctly considered to be zero for each sample in which case the KAE relation shown in Eq. (2) can be simplified to:

$$(1 - X_{rel}) = \exp[-(k't)^n] \quad (3)$$

Approximate values of n e k' can be obtained from a plot of $\log[-\ln(1 - X_{rel})]$ against $\log(t)$ (Table 1).

It can be observed that the derived values of the Avrami exponent are comprised in the range 2.2–2.5 with the only exception of sample_2 with a value of 1.7 related to the very small initial crystallinity. Fractional values of the Avrami index are typical of this analysis the origin being related to the use of a regression applied to a double log scaling of data (experimental uncertainties at short and long times are indeed amplified). On the other hand the expected value of this parameter for a spherulitic growth should be an integer number. A best fitting procedure of the parameters of Eq. (3) to the same data (i.e. without double logarithmic scaling of the crystallinity) by direct integration of Eq. (3) with a value of 3 for the Avrami index was adopted in order to obtain more accurate values of the parameters of the KAE equation, the resulting value of the kinetic constant, k', are reported in Table 2. With the only exception of sample_2, the agreement with data that the predictions of this last procedure show is improved, moreover it is the best one can achieve among the reasonable integer values of n, i.e. 2, 3, 4. This procedure essentially agrees with the assumption of a three-dimensional growth starting from predetermined nuclei: indeed several authors have reported spherulitic type of growth in PET during isothermal crystallization. Douillard et al. [20] at crystallization temperatures between 200 and 235 °C, Jabarin between 110 and 130 °C [21], and between 170 and 225 °C [22] and Verhoyen et al. [19] in their mathematical modeling have imposed a three-dimensional growth during primary crystallization of PET. Values obtained in this way are given in Table 2. Note that these kinetic constants are much more higher than those obtained by the linear regression.) In Fig. 6 the result of this fitting shows that significant deviations can be found mostly for sample_2 according to its initial low crystallinity level. However, the overall good agreement between the model and the experimental data can be appreciated from the plot of X_{rel} vs. $t/t_{0.5}$ (Fig. 7) where all the curves are represented by a single master curve.

Table 2
Parameters of the Avrami equation from best fitting

Sample name	n	k'	k (min^{-1})	$t_{1/2}$ (min)
Sample_2	3	0.0944	0.1067	9.4
Sample_6	3	0.0670	0.0757	13.2
Sample_11	3	0.0602	0.0680	14.7
Sample_20	3	0.0547	0.0618	16.2
Sample_150	3	0.0404	0.0456	21.9
Sample_1500	3	0.0398	0.0450	22.2

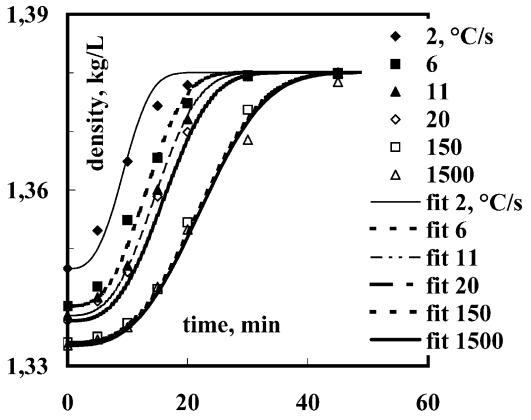

Fig. 6. Comparison of calculated (drawn curves using Eq. (3)) and experimental density data during isothermal crystallization of PET (T_c = 100 °C).

On the other hand, the dependence of the kinetic constant on cooling rate can be obtained based on the relationship between the kinetic constant k and the nucleation and the growth rates after introducing the following simplifying assumptions:

The nucleation is predetermined ($dN/dt = 0$, $N_0 \neq 0$);

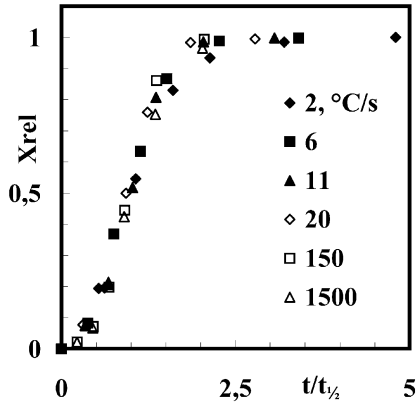

Fig. 7. Plot of relative crystallinity, X_{rel} vs. $t/t_{1/2}$ for the data of Fig. 6.

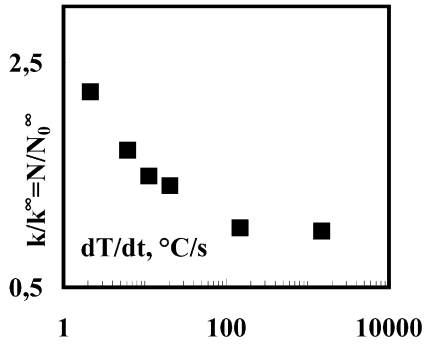

Fig. 8. Variation of number of nuclei as a function of cooling rate using Eq. (4) (see text).

Therefore, N_0 will only be a function of the cooling rate at which the sample is solidified and, hence, is a constant for the single samples ($N_{0i} = \text{constant}$).

The growth rate G, which is a function of T, will be the same for all samples since the crystallization is carried out at the same constant temperature.

Thus, for the ith sample crystallized from the glass, the kinetic constant will be given by:

$$k_i' = \text{const} \times N_{0i}(\mathrm{d}T/\mathrm{d}t)_i \times G(T) \quad (4)$$

Therefore, it can be seen that the ratio of the kinetic constants of two samples having different initial structure, is proportional to the ratio of their initial number of nuclei and as a result a relationship can be obtained between this ratio and the cooling rate. This approach implies that the precrystalline phase acts as a prenucleation site for the formation of the nuclei and subsequently the stable crystalline phase. As is evident from Fig. 8, the number of nuclei (and hence the kinetic constant) decreases with increasing cooling rate, and assumes a constant value above ~100 °C/s, indicated as N_0^{∞}. Under these circumstances the kinetic constant assumes its minimum value k^{∞}. Therefore, the differences in crystallization rate can also be explained in terms of differences in nucleation density.

However, the question still remains, whether such nucleation density difference is representative of the relative number of nuclei effectively frozen upon quenching. Fig. 9 comparatively shows the dependence of microhardness and WAXS patterns on density for the as-quenched and the isothermally crystallized samples. The superposition of the WAXS patterns with the amorphous halo illustrates the region where the amorphous samples are located. Note that the starting samples, whose crystallization kinetics is compared in Fig. 6, are restricted to the 'amorphous' interval. This region corresponds to a rather small density variation while the microhardness exhibits, in contrast, a very large variation range of values which might be related to wide differences in internal order, that are precursors of the final crystalline states [9,10]. However, in spite of such a wide range of 'morphologies' the result obtained for the ratio of nucleation density (Fig. 8) seems to be rather

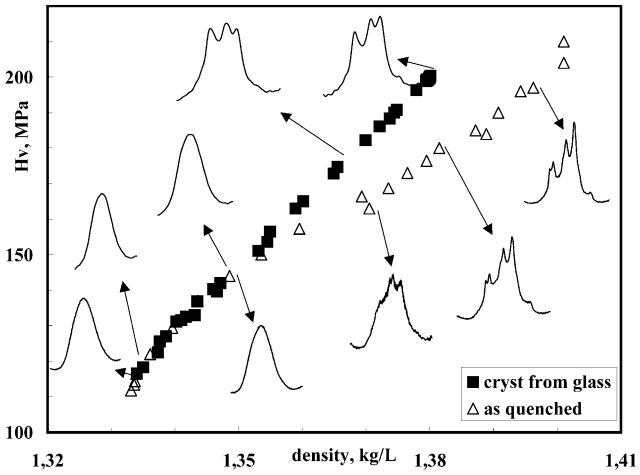

Fig. 9. Microhardness dependence on density for as-quenched samples (open symbols) and after annealing at 100 °C. Selected WAXS patterns are also shown for given conditions (see text).

small. Moreover, one may argue that the ratio shown in Fig. 8 effectively refers to the stable nuclei at the isothermal crystallization temperature, the other clusters, being smaller than the critical nuclei dimensions, should have rapidly dissolved. Thus, although, most of the physical cross-links significantly contribute to the mechanical properties (microhardness), they only influence to a moderate extent the nucleation density since their size is smaller than the critical dimensions at 100 °C. Assuming a value of 27 erg/cm^2 for the average surface energy at the crystal–amorphous boundary, a value of 553 K for the equilibrium melting temperature and a value of 1.8×10^9 erg/cm^3 for the enthalpy of crystallization [23], a figure of ca. 1 nm is obtained for the radius of nuclei of critical dimensions at 100 °C.

Furthermore, Fig. 9 shows that the trend in microhardness is different for the two series of samples except for lower density values, i.e. for the amorphous samples, as revealed by the superimposed WAXS patterns. On the other hand, for the crystalline samples one observes larger microhardness and more disordered WAXS patterns (at the same values of density, of course) for the samples annealed at 100 °C as compared to the as-quenched ones. From this result one could speculate that another mechanism takes place during isothermal crystallization, a mechanism in which physical cross-links having dimensions smaller than the critical nucleus size would become dissolved in the intervening amorphous phase, some of them may even become trapped due to the very low segmental diffusivity of the amorphous phase in the physically cross-linked rubbery state. That this indeed could be the case is shown by the lower density and broader WAXS patterns observed for the samples annealed with respect to the as-quenched ones.

Although this hypothesis is sound a more systematic investigation on the influence of crystallization temperature and polymer molecular weight is being carried out to analyze its consequences.

4. Conclusions

1. The structure of glassy amorphous PET samples depends on the cooling rate used to quench the samples from the melt. Differences in cooling rate used in obtaining a glassy PET sample from the melt induced differences in the inner structure of the glassy samples.
2. The initial structural differences cause differences in crystallization rate from the glass. The reason why some samples crystallize faster than others under the same experimental conditions can be explained in terms of differences in the initial inner structure of the glass.
3. A unique growth mechanism ($n = 3$) accurately describes the cold crystallization process of the samples.
4. The best fitting procedure provides values of the kinetic constant that are more precise.
5. The nucleation density (and the kinetic constant) decreases with increasing cooling rate and becomes constant above $\sim$100 °C/s. For values lower than $\sim$100 °C/s, the nucleation density depends on cooling rate.
6. The differences observed in crystallization rate can be explained in terms of differences in nucleation density.
7. Whether the preformed clusters are acting as nuclei, or some, or most of them, (the precrystalline phase) just restrict the molecular mobility acting as physical cross-links still is an open question.

Acknowledgements

Grateful acknowledgment is due to MCYT (grant BFM2000-1474), Spain, for the support of this investigation. This work has also been supported by EU BRITE project Decrypo contract BRPR.CT96.0147 and by the Italian MURST PRIN99 project. Thanks are also due to the University of Palermo for the support in international exchanges. The SAXS experiments carried out at the synchrotron facilities, beamline A2 of HASYLAB, DESY, Hamburg under projects I95-74 EC and II-01-001 EC were funded by the IHP-Contract HPRI-CF-1999-00040 of the European Community.

References

[1] Van Antwerpen F, Van Krevelen DW. J Polym Sci, Polym Phys 1972;10:2423.
[2] Jabarin SA. J Appl Polym Sci 1987;34:85.
[3] Günther B, Zachmann HG. Polymer 1983;24:1008.
[4] Asano T, Zdeick-Pickuth A, Zachmann HG. J Mater Sci 1989;24:1967.
[5] Baltá-Calleja FJ, Santa Cruz C, Asano T. J Polym Sci, Polym Phys 1993;31:557.
[6] Bove L, D'Aniello C, Gorrasi G, Guadagno L, Vittoria V. Polym Bull 1997;38:579–85.
[7] Varma P, Lofgren EA, Jabarin SA. Polym Engng Sci 1998;38:237.
[8] Piccarolo S, Brucato V, Kiflie Z. Polym Engng Sci 2000;40:1263.
[9] Baltà-Calleja FJ, Garcia MC, Rueda DR, Piccarolo S. Polymer 2000;41:4143.
[10] Rueda DR, Garcia MC, Baltá-Calleja FJ, Piccarolo S. Submitted for publication.
[11] Santa Cruz C, Baltá-Calleja FJ, Zachmann HG, Stribeck N, Asano T. J Polym Sci, Part B: Polym Phys 1991;29:819.
[12] Imai M, Mori K, Mizukami T, Kaji K, Kanaya T. Polymer 1992;33:4451.
[13] Ryan JA, Terrill JN, Fairclough JPA. ACS PMSE Prepr 1999;81:353.
[14] Garcia MC, Rueda DR, Baltá-Calleja FJ. Polym J 1999;31:806.
[15] Wang ZG, Hsiao BS, Kopp C, Sirota EB, Agarwal P, Srinivas S. ACS PMSE Prepr 1999;81:355.
[16] Kolmogoroff AN. Izv Akad Nauk SSR, Ser Math 1937;1:335.
[17] Avrami M. J Chem Phys 1939;7:1103.
[18] Evans UR. Trans Faraday Soc 1945;41:365.
[19] Verhoyen O, Dupret F, Legras R. Polym Engng Sci 1998;38:1594.
[20] Douillard A, Dumazet Ph, Chabert B, Guillet J. Polymer 1993;34:1702.
[21] Jabarin SA. Polym Engng Sci 1989;29:1259.
[22] Jabarin SA. J Appl Polym Sci 1987;34:85.
[23] Ziabicki A. Colloid Polym Sci 1996;274:705.